Onset of Deconfinement in Nucleus-Nucleus Collisions

Marek Gaździcki,[1] Mark I. Gorenstein,[2] and Peter Seyboth[3]

[1] *Institut für Kernphysik, University of Frankfurt, Frankfurt, Germany and Jan Kochanowski University, Kielce, Poland*

[2] *Bogolyubov Institute for Theoretical Physics, Kiev, Ukraine and Frankfurt Institute for Advanced Studies, Frankfurt, Germany*

[3] *Max-Planck-Institut fuer Physik, Munich, Germany*

The energy dependence of hadron production in relativistic nucleus-nucleus collisions reveals anomalies – the *kink, horn*, and *step*. They were predicted as signals of the deconfinement phase transition and observed by the NA49 Collaboration in central PbPb collisions at the CERN SPS. This indicates the onset of the deconfinement in nucleus-nucleus collisions at about 30 AGeV.

1. INTRODUCTION

One of the important issues of contemporary physics is the understanding of strong interactions and in particular the study of the properties of strongly interacting matter in equilibrium. What are the phases of this matter and what do the transitions between them look like? These questions motivate broad experimental and theoretical efforts since more than 40 years. In particular, the advent of the quark model of hadrons and the development of the commonly accepted theory of strong interactions, quantum chromodynamics, naturally led to expectations that matter at very high densities may exist in a state of quasi-free quarks and gluons, the quark-gluon plasma (QGP) [1–3].

A transition between the deconfined and the confined phase of strongly interacting matter probably took place during the expansion and cooling of the early Universe, about 1 microsecond after the Big Bang. Cosmological signatures of this transition are difficult to identify today. However, extremely dense strongly interacting matter fills the interior of neutron stars. Arguments in favor of the existence of quark matter in the center of such stars were advanced soon after formulation of the quark hypothesis. One of the pioneering papers [2] argued: "A neutron has a radius of about 0.5–1 fm (1 fm = 10^{-15} m), and so has a density of about 8×10^{14} g/cm^3, whereas the central density of a neutron star can be as much as 10^{16}–

10^{17} g/cm^3. In this case, one must expect the hadrons to overlap, and their individuality to be confused. Therefore, we suggest that matter at such densities is a quark soup." The creation of matter in a deconfined phase, i.e. in the QGP phase, may be the only possibility to 'see' quarks and gluons moving freely in a large volume.

Cosmological and astrophysical objects with the required properties are, unfortunately, difficult to investigate. Systematic study of the properties of strongly interacting matter requires a method to create it under well controlled conditions in the laboratory. The study of collisions of two heavy nuclei gives us this possibility. Such a collision produces a droplet of strongly interacting matter of high energy density, the so-called fireball.

Experimental searches for QGP signals started at the Super Proton Synchrotron (SPS) of the European Organization for Nuclear Research (CERN) and the Alternating Gradient Synchrotron (AGS) of Brookhaven National Laboratory (BNL) in the mid 1980s. Today they are pursued also at much higher collision energies at the Relativistic Heavy Ion Collider (RHIC) at BNL. The experiments on nucleus-nucleus (AA) collisions at the Large Hadron Collider (LHC) in CERN join the world effort at energies 20 times higher than at RHIC. Most probably QGP is formed at the early stage of heavy ion collisions at the top SPS energy and at RHIC energies. Unambiguous evidence of the QGP state is difficult to obtain because of the lack of unique and quantitative predictions of the expected QGP signals from the theory of strong interactions (QCD). For this reason the NA49 Collaboration at the CERN SPS has searched over the past years for signs of the onset of QGP creation in the energy dependence of hadron production properties. This search was motivated by the statistical model of the early stage (SMES) [4], showing that the onset of deconfinement should lead to rapid changes of the energy dependence of numerous experimentally detectable properties of the collisions, all appearing in a common energy domain. The energy scan programme of the NA49 Collaboration recorded central PbPb collisions at several energies: 20, 30, 40, 80, and 158 AGeV [5]. The predicted features have been observed and new experiments now continue detailed studies in the energy region of the onset of deconfinement. In this paper we review the experimental and theoretical status of the onset of deconfinement (more details can be found in Ref. [6]). The basic qualitative ideas are presented and the SMES signals of deconfinement are discussed and compared with the latest experimental results.

2. ENERGY SCAN PROGRAMME

Phase transitions are fascinating physical phenomena. Small changes in temperature or pressure lead to dramatic changes in macroscopic properties of matter. Common examples from our daily life are transitions between solids, liquids and gases like boiling and freezing of water. The well known phase diagram of water is shown in Fig. 1, where the regions of existence of the various phases of water are depicted in a diagram of pressure and temperature. When adding heat to water one increases its temperature moving through its different phases and crossing their boundaries, as indicated by the dashed arrow in Fig. 1 for the example of constant atmospheric pressure. Dependence of the water temperature on the amount of added heat, called the heating curve of water, is shown in Fig. 2. In pure phases, such as ice, water or vapor, the temperature increases monotonically with added heat. The two regions of constant temperature (steps) signal the ice-water and water-vapor phase transitions. In these mixed phase regions added heat is used for the phase transformation instead of the increase of temperature as in the pure phase regions.

There are three parameters which describe the thermodynamical properties of a system. In non-relativistic systems they are temperature, particle number density, and pressure. The equation of state connects them, e.g., the pressure is a well defined function of temperature and particle density for a specific substance. In experiments on water one can most easily fix temperature and pressure to define the point on the phase diagram shown in Fig. 1. Unlike in water, the number of particles is not conserved in strongly interacting relativistic matter. Instead of the particle number density the baryonic number, i.e. the difference between the number of baryons and anti-baryons, is conserved. In calculations it is convenient to use the equivalent variables baryonic number density or baryonic chemical potential. The phase diagram of strongly interacting matter emerging from theoretical considerations and experimental results is shown in Fig. 3 in terms of the commonly used quantities temperature and baryonic chemical potential. Laboratory experiments (see discussion below) can create strongly interacting matter with different temperatures T and baryonic chemical potentials μ_B. The functional dependence of the pressure on T and μ_B, i.e. the equation of state of strongly interacting matter, remains the subject of intense experimental and theoretical studies.

It is natural to expect that with increasing collision energy the fireball energy density also

increases. Thus like in the case of water heating and observing successive transitions between its phases, we hope that with increasing collision energy we can detect anomalies in the energy dependence of hadron production properties and thus discover successive transitions between various phases of strongly interacting matter created at the early stage of collisions. The arrow in Fig. 3 schematically traces the position of the initially created fireball on the phase diagram when the energy of nucleus-nucleus collisions is increasing. At sufficiently high collision energy this matter droplet may reach the QGP phase (see Fig. 3). The life time of the fireball is very short, about 10^{-22} seconds. It quickly expands, cools down (see Fig. 4) and finally decays into hadrons and a few light nuclei. These decay products are measured in detectors surrounding the collision point.

The first phase transition of strongly interacting matter was observed studying collisions at very low energies [7] ($\sqrt{s_{\rm NN}} < 2$ GeV, where $\sqrt{s_{\rm NN}}$ is the c.m.s. energy of the nucleon pair). This transition between a nuclear liquid and a nuclear gas happens at a temperature of about 6×10^{10} K (5 MeV). The phase transition line and critical point M lie at large μ_B and small T inside the hadron phase region of the phase diagram as shown in Figs. 3 and 4. Emerging results from the study of high energy collisions of nuclei confirm the existence of the second phase transition in strongly interacting matter. It is the so–called deconfinement phase transition.

The dependence of the early stage temperature T on the collision energy in SMES is shown in Fig. 5*a*. Outside the transition region T increases with F, Fermi's energy measure defined in Eq. (1). Inside the transition region T is constant. The fraction of the volume occupied by the QGP at the early stage of central AA collision increases rapidly in the transition region, as shown in Fig. 5*b*.

3. THE KINK, HORN, AND STEP

The majority of all particles produced in high energy interactions are pions. Thus, pions carry basic information on the entropy created in the collisions. On the other hand, entropy production should depend on the form of matter present at the early stage of collisions. Deconfined matter is expected to lead to a final state with higher entropy than that created by confined matter. Consequently, it is natural to expect that the onset of creation of deconfined matter should be signaled by an enhancement of pion production. This intuitive

argumentation can be quantified within SMES assuming the generalized Fermi–Landau initial conditions: the initial volume is Lorenz-contracted, $V \propto \langle N_W \rangle \cdot (\sqrt{s_{NN}})^{-1}$ where $\langle N_W \rangle$ is the mean number of wounded nucleons (i.e. the number of nucleons participating in inelastic AA reactions). A trivial dependence of the pion multiplicity on the size of colliding nuclei should be removed and thus the relevant quantity is the ratio of the mean pion multiplicity $\langle \pi \rangle$ to $\langle N_W \rangle$. The initial energy density is given by $\varepsilon \propto gT^4 \propto (\sqrt{s_{NN}} - 2m_N) \cdot \sqrt{s_{NN}}$, where g is an effective number of internal degrees of freedom at the early stage and m_N is the nucleon mass. The pion multiplicity is proportional to the initial entropy, and the $\langle \pi \rangle / \langle N_W \rangle$ ratio can be thus calculated outside the transition region as:

$$\frac{\langle \pi \rangle}{\langle N_W \rangle} \propto \frac{VgT^3}{\langle N_W \rangle} \propto \frac{g^{1/4}(\sqrt{s_{NN}} - 2m_N)^{3/4}}{(\sqrt{s_{NN}})^{1/4}} \equiv \; g^{1/4} F. \tag{1}$$

Therefore, the $\langle \pi \rangle / \langle N_W \rangle$ ratio increases linearly with Fermi's energy measure F outside the transition region, and the slope parameter is proportional to $g^{1/4}$ [8]. In the transition region, a steepening of the pion energy dependence is predicted, because of the activation of partonic degrees of freedom, i.e. the effective number of internal degrees of freedom in the QGP is larger than in the hadron gas (HG): $g_{\rm QGP} > g_{\rm HG}$.

A compilation of data on the pion multiplicity produced in central PbPb (AuAu) collisions and $pp(\bar{p})$ interactions is presented in Fig. 6*a* for data available in 1998, and Fig. 6*b* for presently available results [5]. The mean pion multiplicity $\langle \pi \rangle = 1.5\,(\langle \pi^- \rangle + \langle \pi^- \rangle)$ per wounded nucleon is plotted as a function of F. Results from $pp(\bar{p})$ interactions are shown by the open symbols those from central PbPb (AuAu) collisions by the filled symbols. Up to the top SPS energy the mean pion multiplicity in pp interactions is approximately proportional to F. A fit of $\langle \pi \rangle / \langle N_W \rangle = bF$ yields a value of $b \cong 1.063$ GeV$^{-1/2}$. For central PbPb and AuAu collisions the energy dependence is more complicated. Below 40 AGeV the ratio $\langle \pi \rangle / \langle N_W \rangle$ is lower in AA collisions than in $pp(\bar{p})$ interactions (pion suppression) while at higher energies this ratio is larger in AA collisions than in $pp(\bar{p})$ interactions (pion enhancement). A linear fit, $\langle \pi \rangle / \langle N_W \rangle = a + bF$ for $F < 1.85$ GeV$^{1/2}$, gives $a \cong -0.45$ and $b \cong 1.03$ GeV$^{-1/2}$. The slope parameter fitted in the range $F > 3.5$ GeV$^{1/2}$ is $b \cong 1.33$. This is shown by the solid line in Fig. 6 (the lowest point at the top RHIC energy was excluded from the fit). Thus, in the region 15–40 AGeV between the highest AGS and the lowest SPS energy the slope increases by a factor of about 1.3. This increase of the slope for AA collisions is interpreted within SMES as due to an increase of the effective number of the internal degrees of freedom

by a factor of $g_{\rm QGP}/g_{\rm HG} = (1.3)^4 \cong 3$ [4, 8]. It is caused by the creation of a transient state of deconfined matter at collision energies higher than 30 AGeV.

The energy dependence of the strangeness to entropy ratio is a crucial signal of deconfinement. The temperature dependence of the multiplicity of a particle is strongly dependent on its mass,

$$\langle N_i \rangle \;=\; \frac{g_i V}{2\pi^2}\; m_i^2 T\; K_2\left(\frac{m_i}{T}\right)\;, \qquad (2)$$

where g_i and m_i are respectively the degeneracy factor and particle mass, and K_2 is the modified Hankel function. For light hadrons ($m_l/T \ll 1$) one finds from Eq. (2), $\langle N_l \rangle \propto T^3$, whereas for heavy hadrons ($m_h/T \gg 1$) Eq. (2) leads to $\langle N_h \rangle \propto T^{3/2} \exp(-\, m_h/T)$. Within SMES at low collision energies, when HG matter is produced, the strangeness to entropy ratio increases steeply with collision energy. This is due to the low temperature at the early stage and the high mass of the carriers of strangeness (the kaon mass), i.e. $m_K \gg T$ and the total strangeness is proportional to $T^{3/2} \exp(-\, m_K/T)$. On the other hand, the total entropy (approximately $\propto \langle \pi \rangle$) is approximately proportional to T^3. Therefore, the strangeness to pion ratio is approximately $T^{-3/2} \exp(-m_K/T)$ in the confined matter and increases strongly with the collision energy. When the transition to deconfined matter is crossed, the mass of the strangeness carriers decreases significantly to $m_s \cong 150$ MeV, the strange quark mass. Due to the low mass ($m_s < T$) the strangeness yield becomes approximately proportional to the entropy (both are proportional to T^3), and the strangeness to entropy (or pion) ratio in the QGP becomes independent of collision energy. This leads to a "jump" in the energy dependence from the larger value for confined matter to the value for deconfined matter. Thus, within SMES, the non-monotonic energy dependence of the strangeness to entropy ratio is followed by a saturation at the value for deconfined matter as a direct consequence of the onset of deconfinement taking place at about 30 AGeV [4]. This is illustrated by Fig. 7.

One can argue that the strangeness to entropy ratio is closely proportional to the two ratios directly measured in experiments: the $\langle K^+ \rangle / \langle \pi^+ \rangle$ ratio and the $E_s = (\langle \Lambda \rangle + \langle K + \overline{K} \rangle)/\langle \pi \rangle$ ratio. The energy dependence of these full phase space ratios is plotted in Fig. 8 for central PbPb (AuAu) collisions and pp interactions.

Kaons are the lightest strange hadrons and $\langle K^+ \rangle$ accounts for about half of all the anti-strange quarks produced in PbPb collisions at AGS and SPS energies. K^+ and K^0 carry the dominant fraction of all produced $\overline{s}$-quarks exceeding 95% in PbPb collisions at 158 AGeV

if the small contribution of hidden strangeness mesons is neglected. Because $\langle K^+ \rangle \cong \langle K^0 \rangle$ in approximately isospin symmetric collisions of heavy nuclei, the K^+ yield is nearly proportional to the total strangeness production and only weakly sensitive to the baryon density. As a significant fraction of s-quarks (about 50% in central PbPb collisions at 158 AGeV) is carried by hyperons, the number of produced anti-kaons, K^- and $\overline{K}^0$, is sensitive to both the strangeness yield and the baryon density. In the E_s ratio all main carriers of strange and anti-strange quarks are included. The neglected contribution of $\overline{\Lambda}$ and other hyperons and anti-hyperons is about 10% at SPS energies. Both the $\langle K^+ \rangle / \langle \pi^+ \rangle$ and E_s ratios are approximately, within 5% at SPS energies, proportional to the ratio of total multiplicity of s and $\overline{s}$ quarks to the multiplicity of pions. It should be noted that the $\langle K^+ \rangle / \langle \pi^+ \rangle$ ratio is expected to be similar (within about 10%) for pp, np, and nn interactions at 158 AGeV, whereas the E_s ratio is independent of the isospin of the initial state in nucleon-nucleon interactions.

For pp interactions both ratios show monotonic increase with energy. However, very different behavior is observed for central PbPb (AuAu) collisions. The steep threshold rise of the ratios characteristic for confined matter then settles into saturation at the level expected for deconfined matter. In the transition region (at low SPS energies) a sharp maximum is observed caused by the higher strangeness to entropy ratio in confined matter as compared to deconfined matter. As seen in Fig. 8 the measured dependence is consistent with that predicted within SMES [4].

The energy density at the early stage increases with increasing collision energy. At low and high energies, when a pure confined or deconfined phase is produced, this leads to an increase of the initial temperature and pressure. This, in turn, results in an increase of the transverse expansion of the matter and consequently a flattening of the transverse mass spectra of final state hadrons. One expects an 'anomaly' [9–11] in the energy dependence of the transverse hadron activity as the temperature and pressure are approximately constant in the mixed phase.

Experimental data on spectra of the transverse mass $m_T = (m^2 + p_T^2)^{1/2}$ are usually parametrized by a simple exponential dependence:

$$\frac{dN}{m_T dm_T} \propto \exp\left(-\frac{m_T}{T^*}\right) . \tag{3}$$

The inverse slope parameter T^* is sensitive to both the thermal and collective motion in

the transverse direction. Hydrodynamic transverse flow with collective velocity v_T modifies the Boltzmann m_T-spectrum of hadrons. At low transverse momenta, it leads to the result $T^*_{\rm low-p_T} \cong T_{\rm kin} + \frac{1}{2} m\ v_T^2$, where T_{kin} is the kinetic freeze-out temperature. A linear mass dependence of T^* is supported by the data for hadron spectra at small p_T. However, for $p_T \gg m$ the hydrodynamic transverse flow leads to a mass-independent blue-shifted 'temperature': $T^*_{\rm high-p_T} = T_{\rm kin}\ [(1+v_T)/(1-v_T)]^{1/2}$. Note that a simple exponential fit (3) neither works for light π-mesons, $T^*_{\rm low-p_T}(\pi) < T^*_{\rm high-p_T}(\pi)$, nor for heavy (anti)protons and (anti)lambdas, $T^*_{\rm low-p_T}(p,\Lambda) > T^*_{\rm high-p_T}(p,\Lambda)$ (see e.g., Refs. [12, 13]).

Kaons are the most suitable measured hadron species for observing the effect of the modification of the equation of state due to the onset of the deconfinement in hadron transverse momentum spectra. The arguments are the following [11]: 1) the kaon m_T–spectra are only weakly affected by hadron re-scattering and resonance decays during the post-hydrodynamic hadron cascade at SPS and RHIC energies; 2) a simple one parameter exponential fit (3) is quite accurate for kaons in central AA collisions at all energies, i.e. $T^*_{\rm low-p_T}(K) \approx T^*_{\rm high-p_T}(K)$ for kaons; 3) high quality data on m_T-spectra of K^+ and K^- mesons in central PbPb and AuAu collisions are available in the full range of relevant energies. Thus, one expects [11] that T^* for kaons increases when either pure confined or deconfined phase is produced at the early stage of AA collision, whereas T^* remains approximately constant when the initial matter is in a mixed phase state.

The energy dependence of the inverse slope parameter fitted to the K^+ and K^- transverse mass spectra for central PbPb (AuAu) collisions is shown in Fig. 9. The striking features of the data can be summarized and interpreted as follows. The T^* parameter increases strongly with collision energy up to the SPS energy point 30 AGeV. This is an energy region where the creation of confined matter at the early stage of the collisions is expected. Increasing collision energy leads to an increase of the early stage temperature (see Fig. 5*a*) and pressure. Consequently the transverse activity of produced hadrons, measured by the inverse slope parameter, increases with increasing energy. The T^* parameter is approximately independent of the collision energy in the SPS energy range 30–158 AGeV. In this energy region the transition between confined and deconfined matter is expected to occur. The resulting modification of the equation of state "suppresses" the hydrodynamic transverse expansion and leads to the observed plateau structure in the energy dependence of the T^* parameter [11, 14]. At higher energies (RHIC data), T^* again increases with the collision energy. The equation

of state at the early stage becomes again stiff, the early stage temperature and pressure increase with collision energy resulting in a renewed rise of T^*. The parameter T^* appears to increase smoothly in pp interactions as shown in the left panel of Fig. 9.

For the transverse mass spectra of pions and protons the inverse slope parameter depends on the transverse mass interval used in the fit. The mean transverse mass $\langle m_T \rangle$ provides an alternative characterization of the m_T-spectra. The energy dependence of $\langle m_T \rangle - m$ for pions, kaons and (anti)protons is shown in Fig. 10. The results shown in Fig. 10 demonstrate that the approximate energy independence of $\langle m_T \rangle$ in the SPS energy range is a common feature for all particles investigated.

4. LONGITUDINAL COLLECTIVE FLOW

The collective flow of matter at freeze-out depends on the properties of the early stage as well as on the expansion dynamics itself. Within SMES the collision energy dependence of the early stage properties is predicted. In particular, in the energy range in which the mixed phase is created the pressure and temperature are constant and at the end of the mixed phase domain the pressure to energy density ratio reaches its minimum (the softest point of the EoS). From general hydrodynamic considerations this is expected to lead to a reduction of the build-up of transverse flow [11]. Similar effects are seen for longitudinal collective flow [15] within Landau's hydrodynamic model [16, 17]. The interest in this model was revived by the remarkable observation that the rapidity distributions at all investigated energies can be well described by a single Gaussian. (see [5] and references therein). Moreover, the energy dependence of the width can also be described reasonably well by the same model.

The main physics assumptions of Landau's picture are as follows. The collision of two Lorentz-contracted nuclei leads to a complete stopping of the colliding nuclei and full thermalization of the created hadronic matter. This establishes the volume and energy density for the initial conditions of hydrodynamic expansion at each collision energy. Assuming for simplicity the equation of state in the form $p = c_s^2 \varepsilon$ (where p and ε correspond to the pressure and energy density, respectively, and c_s denotes the speed of sound with $c_s^2 = 1/3$ for an ideal massless particle gas) the pion rapidity spectrum is given by:

$$\frac{dN_\pi}{dy} = \frac{K s_{\rm NN}^{1/4}}{\sqrt{2\pi\sigma_y^2}} \exp\left(-\frac{y^2}{2\sigma_y^2}\right) \tag{4}$$

with

$$\sigma_y^2 \;=\; \frac{8}{3}\frac{c_s^2}{1-c_s^4}\,\ln(\sqrt{s}_{\rm NN}/2m_{\rm N}) \quad , \tag{5}$$

where K is a normalization factor converting entropy to pion density [1].

Eqs. (4)–(5) with $c_0^2 = 1/3$, only roughly reproduce the measured dependence of σ_y^2 on the collision energy. At low AGS energies and at the top RHIC energy, the experimental points are under-predicted, while in the SPS energy regime Landau's model over-predicts the width of the rapidity distributions. These deviations can be attributed to the changes in the equation of state, which can be effectively parametrized by allowing the speed of sound to be dependent on collision energy. By inverting Eq. (5) one can express c_s^2 as a function of the measured width of the rapidity distribution:

$$c_s^2 \;=\; \sqrt{\left[\frac{4\ln(\sqrt{s}_{\rm NN}/2m_{\rm N})}{3\sigma_y^2}\right]^2+1} \;-\; \frac{4\,\ln(\sqrt{s}_{\rm NN}/2m_p)}{3\sigma_y^2}\,. \tag{6}$$

The energy dependence of the sound velocities extracted from the data using Eq. (6) was obtained in Ref. [15] and is presented in Fig. 11*a*. The sound velocities exhibit a clear minimum (usually called the softest point) around a beam energy of $\sqrt{s_{\rm NN}} = 7.6$ GeV (30 AGeV). As discussed previously the weakening of the transverse and longitudinal expansion is expected within SMES at low SPS energies due to the onset of deconfinement which softens the EoS at the early stage. Generally, a softening of the equation of state was predicted as a signal for the mixed phase at the transition energy from hadronic to partonic matter. Therefore, we conclude that the data on rapidity spectra of negatively charged pions are indeed compatible with the assumption of the onset of deconfinement at the low SPS energies.

5. EVENT-BY-EVENT FLUCTUATIONS

Up to this point only quantities averaged over many collisions (events) were considered. Next an extension of SMES is reviewed which leads to predictions of fluctuations from event to event. The key additional assumption is that when the collision energy is fixed, the energy, which is used for particle production (inelastic energy) can still fluctuate. These dynamical energy fluctuations lead to dynamical fluctuations of macroscopic properties X

[1] Note that Eq. (5) is obtained assuming that c_s depends only on the early stage energy density and its dependence on decreasing energy density during expansion is neglected. This assumption needs clarification by future studies

of the matter, like its entropy and strangeness content. The relation between them is given by the EoS. For example, different values of the energy of the early equilibrium state lead to different, but uniquely determined, entropies. Since the EoS shows an anomalous behavior in the phase transition region, this anomaly should also be visible in the ratio of entropy to energy fluctuations [18].

According to the first and the second principles of thermodynamics the entropy change δS is given as $T\delta S = \delta E + p\delta V$. For central AA collisions, one expects $\delta V \cong 0$. Within SMES the ratio of entropy to energy fluctuations can then be calculated and expressed as a simple function of the p/ε ratio [18]:

$$R_e \equiv \frac{(\delta S)^2/S^2}{(\delta E)^2/E^2} = \left(1 + \frac{p}{\varepsilon}\right)^{-2} . \tag{7}$$

Within the SMES model, confined matter (which is modeled as an ideal gas) is created at the early collision stage below a collision energy of 30 AGeV. In this domain, the ratio p/ε, and consequently the R_e ratio, are approximately independent of the collision energy and equal about 1/3 and 0.56, respectively. The SMES model assumes that the deconfinement phase transition is of the first order. Thus, there is a mixed phase region, corresponding to the energy interval 30–60 AGeV. At the end of this region the p/ε ratio reaches a minimum (the 'softest point' of the EoS. Thus in the transition energy range the R_e ratio increases and reaches its maximum, $R_e \approx 0.8$, at the end of the transition domain. Further on, in the pure deconfined phase, which is represented by an ideal quark-gluon gas under bag pressure, the p/ε ratio increases and again approaches its asymptotic value 1/3 at the highest SPS energy of 160 AGeV. The early stage energy and entropy fluctuations entering Eq. (7) are not directly observable. However, as argued in Ref. [18], they can be inferred from the experimentally accessible information on the final state energy and multiplicity fluctuations.

In Ref. [19] the energy dependence of dynamical strangeness fluctuations caused by dynamical energy fluctuations was studied within the SMES model. Defining $\overline{N}_s$ as the total number of strange quark-anti-quark pairs created in an AA collision one calculates the fluctuation ratio as:

$$R_s = \frac{(\delta\overline{N}_s)^2/\overline{N}_s^2}{(\delta E)^2/E^2} . \tag{8}$$

For $T \to \infty$ the system is in the QGP phase. Strange (anti-)quarks can be considered as massless and the bag constant can be neglected. Then $\varepsilon \propto T^4$ and $n_s \propto T^3$ and consequently $d\varepsilon/\varepsilon = 4dT/T$ and $dn_s/n_s = 3dT/T$, which results in $R_s = (3/4)^2 \cong 0.56$. In the confined

phase, $T < T_c$, the energy density is still approximately proportional to T^4 due to the dominant contributions of non-strange hadrons. However, the dependence of the strangeness density on T is governed by the exponential factor, $n_s \propto \exp(-m_S)$, as $T << m_S = m_W^s \cong$ 500 MeV. Therefore, at small T one finds $d\varepsilon/\varepsilon = 4dT/T$ and $dn_s/n_s = m_S dT/T^2$, so that the ratio $R_s = m_S/(4T)$ decreases with T. The strangeness density n_s is small and goes to zero at $T \to 0$, but the fluctuation ratio R_s Eq. (8) is large and increases to infinity in the zero temperature limit. One finds a non-monotonic energy dependence of R_e with a maximum at the boundary between the mixed phase and the QGP [18]. A pronounced minimum-structure is expected in the dependence of R_s on the collision energy [19]. It is located at $\sqrt{s_{NN}}$ = 7–12 GeV (30–60 AGeV), where the mixed phase is created at the early stage of AA collision.

Both entropy and strangeness fluctuation measures, R_e and R_s, show anomalous behavior in the transition region: a maximum is expected for R_e and a minimum for R_s. Consequently, an even stronger anomaly is predicted for the ratio:

$$R_{s/e} \equiv \frac{R_s}{R_e} = \frac{(\delta\overline{N}_s)^2/\overline{N}_s^2}{(\delta\overline{N}_-)^2/\overline{N}_-^2} , \tag{9}$$

shown in Fig. 7*b*. Experimental measurements of $R_{s/e}$ may be easier than the measurements of R_e and R_s because the ratio $R_{s/e}$ requires measurements of particle multiplicities only, whereas both R_e and R_s involve also measurements of particle energies.

The *tooth* structure in the energy dependence of $R_{s/e}$ shown in Fig. 11*b*, might be seen in the event-by-event fluctuations of the K/π ratio. The energy dependence of the fluctuations of this ratio in central PbPb collisions was studied by NA49 using the so-called $\sigma_{\rm dyn}$ measure [20]. The 'dynamical' K/π fluctuations increase significantly with decreasing energy below 40 AGeV. However, it is unclear whether this increase is related to the rapid increase of the $R_{s/e}$ measure predicted due to the onset of deconfinement at energies below 30 AGeV.

6. CONCLUSIONS

In this review we present the experimental and theoretical status of the evidence for the threshold of quark-gluon plasma creation in high energy nucleus-nucleus interactions. The location in energy of this so-called onset of deconfinement, as well as key experimental signals were predicted by the statistical model of the early stage of the collision process [4].

These signals were searched for and observed within the energy scan program of the NA49 Collaboration at the CERN SPS. Together with measurements at lower (LBL, JINR, SIS, BNL AGS) and higher (BNL RHIC) energies the properties of hadron production in heavy ion collisions were established in a broad energy range. Their energy dependence led to the conclusion that the predicted signals of the onset of deconfinement appear in a common energy domain covered by the SPS at CERN. These features of the data serve as strong experimental evidence for the existence of the onset of deconfinement and thus for the quark-gluon plasma itself.

New experimental programs have started at the CERN SPS and BNL RHIC which are devoted to the study of nucleus-nucleus collisions in the energy region, where the NA49 experiment found evidence for the onset of deconfinement. The STAR experiment at RHIC will provide a necessary confirmation of these results. The new CERN experiment NA61 will address the questions how this observed phenomenon depends on the volume of matter and what the properties of the transition region are.

The onset of deconfinement refers to the beginning of the creation of a deconfined state of strongly interacting matter (ultimately a quark-gluon plasma) at the early stage of nucleus-nucleus collisions when increasing the collision energy. With increasing collision energy the energy density of matter created at the early stage of AA collisions increases. The existence of the onset of deconfinement is the most straightforward consequence of the existence of two phases of strongly interacting matter, i.e. confined matter and QGP. The experimental observation of the onset of deconfinement required a one dimensional scan in collision energy with heavy ions as performed by NA49. All signals of the onset of deconfinement discussed in this paper relate to the difference in properties of confined matter and QGP. They are not sensitive to the structure of the transition region.

Discovery of the onset of deconfinement implies the existence of QGP and of a transition region between confined and QGP phases. Numerous possibilities concerning the structure of the transition region are under discussion. The most popular one claims that a first order phase transition separates both phases in the high baryonic chemical potential domain. In the low baryonic chemical potential domain a rapid crossover is expected. The end point of the first order phase transition line is the critical point.

The characteristic signatures of the critical point can be observed if the freeze-out point is located close to the critical point. The analysis of the existing experimental data indicates

that the location of the freeze-out point in the phase diagram depends on the collision energy and the mass of the colliding nuclei. Thus the experimental search for the critical point requires a two-dimensional scan in collision energy and size of the colliding nuclei. The NA61 experiment [21, 22] at the CERN SPS started this scan in 2009. It should be completed within several years. Note, that a two dimensional scan is actually required for any study of the structure of the transition region, independent of the hypothesis tested.

The energy scan program at the CERN SPS together with measurements at lower (LBL, JINR, SIS, BNL AGS) and higher (BNL RHIC) energies yielded systematic data on the energy dependence of hadron production in central PbPb (AuAu) collisions. Anomalies in the energy dependence of hadron production are seen in central AA collisions which are absent in *pp* reactions. They indicate that the onset of deconfinement in central PbPb collisions is located at about 30 AGeV. The condition that the freeze-out point is near the critical point implies that the early stage of the system is above (or on) the transition line. This in turn means that the optimal energy range for the search for the critical point lies above the energy of the onset of deconfinement. This general condition limits the search for the critical point to the collision energy range $E_{\rm LAB} > 30$ AGeV.

---

1. D. D. Ivanenko and D. F. Kurdgelaidze, Astrophysics **1**, 251 (1965) [Astrofiz. **1**, 479 (1965)].
2. N. Cabibbo and G. Parisi, Phys. Lett. B **59**, 67 (1975);
   J. C. Collins and M. J. Perry, Phys. Rev. Lett. **34**, 1353 (1975).
3. E. V. Shuryak, Phys. Rept. **61**, 71 (1980).
4. M. Gaździcki and M. I. Gorenstein, Acta Phys. Polon. B **30**, 2705 (1999).
5. C. Alt *et al.* (NA49 Collab.), Phys. Rev. C **77**, 024903 (2008).
6. M. Gaździcki, M. I. Gorenstein, and P. Seyboth, arXiv: 1006.1765 [hep-ph].
7. J. Pochodzalla *et al.*, Phys. Rev. Lett. **75**, 1040 (1995).
8. M. Gaździcki, Z. Phys. C **66**, 659 (1995); J. Phys. G **23**, 1881 (1997).
9. L. Van Hove, Phys. Lett. B **118**, 138 (1982).
10. C. M. Hung and E. Shuryak, Phys. Rev. Lett. **75**, 4003 (1995); Phys. Rev. C **57**, 1891 (1997).
11. M. I. Gorenstein, M. Gaździcki, and K. A. Bugaev, Phys. Lett. B **567**, 175 (2003).
12. D. Teaney, J. Lauret, and E. V. Shuryak, Phys. Rev. Lett. **86**, 4783 (2001).

13. M. I. Gorenstein, K. A. Bugaev, and M. Gaździcki, Phys. Rev. Lett. **88**, 132301 (2002); Phys. Lett. B **544**, 127 (2002); Phys. Rev. C **68**, 017901 (2003).
14. M. Gaździcki *et al.*, Braz. J. Phys. **34**, 322 (2004); Acta Phys. Polon. B **35**, 179 (2004).
15. M. Bleicher, arXiv: hep-ph/0509314.
16. L. D. Landau, Izv. Akad. Nauk Ser. Fiz. **17**, 51 (1953).
17. S. Z. Belenkij and L. D. Landau, Nuovo Cim. Suppl. **3S10**, 15 (1956) [Usp. Fiz. Nauk **56**, 309 (1955)].
18. M. Gazdzicki, M. I. Gorenstein, and S. Mrowczynski, Phys. Lett. B **585**, 115 (2004).
19. M. I. Gorenstein, M. Gazdzicki, and O. S. Zozulya, Phys. Lett. B **585**, 237 (2004).
20. C. Alt *et al.* (NA49 Collab.), Phys. Rev. C **79**, 044910 (2009).
21. M. Gazdzicki *et al.* (NA61/SHINE Collab.), PoS CPOD2006, 016 (2006).
22. N. Antoniou *et al.* (NA61/SHINE Collab.), CERN-SPSC-2006-034.

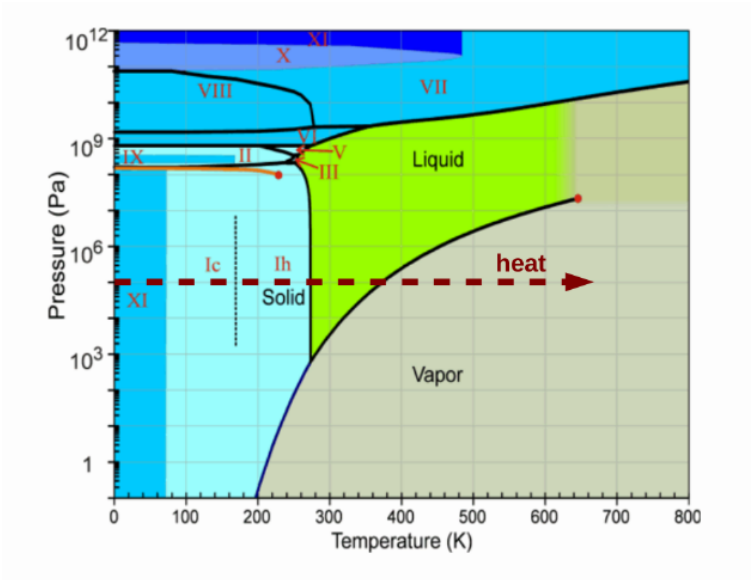

Figure 1. Phases of water. When adding heat (energy) at constant pressure water is transformed from solid to liquid and then from liquid to vapor as indicated by the dashed arrow.

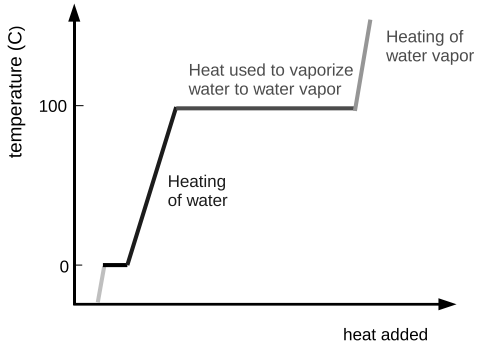

Figure 2. Heating curve of water at fixed atmospheric pressure, corresponding to the trajectory in the phase diagram of water indicated by the dashed arrow in Fig. 1.

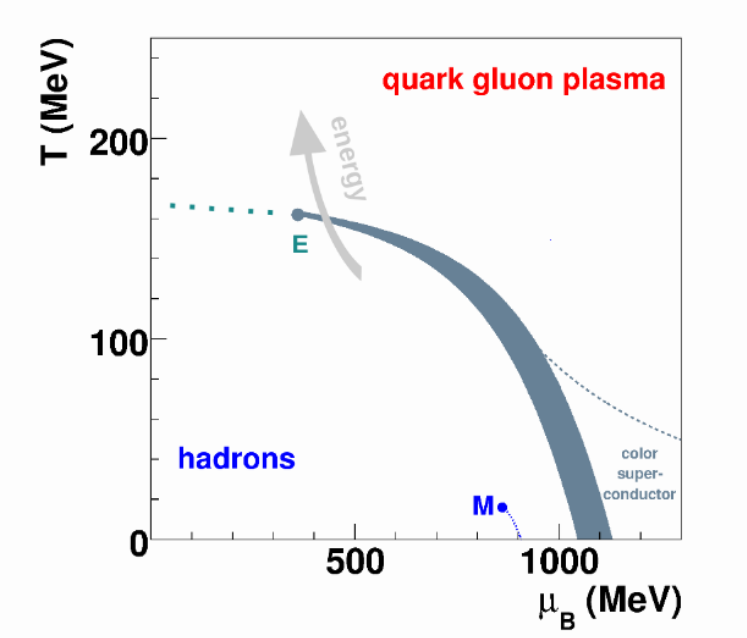

Figure 3. Phases of strongly interacting matter. With increasing collision energy the matter created at the early stage of nucleus-nucleus collisions changes its properties as indicated by the arrow. At low energy it is in the confined phase (hadrons), at sufficiently high energy in the deconfined phase (QGP). M is the critical point of the nuclear liquid-gas phase transition. The shaded band shows the first order phase boundary between the hadron and QGP phase which is expected to end in a critical end point E. At E the sharp phase transition turns into a rapid crossover indicated as the dotted line.

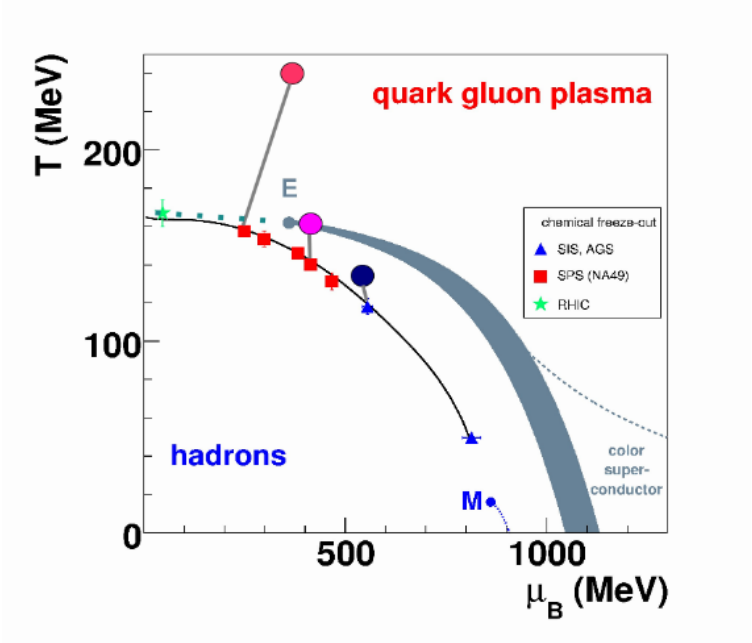

Figure 4. Parameters of strongly interacting matter created at the early stage of nucleus-nucleus interactions are shown by the full circles for central PbPb (AuAu) collisions at the top AGS energy ($\sqrt{s_{\rm NN}} \approx 5.5$ GeV), intermediate SPS energy ($\sqrt{s_{\rm NN}} \approx 7.6$ GeV) and top SPS energy ($\sqrt{s_{\rm NN}} \approx 17$ GeV). The created fireball expands and cools along trajectories indicated by solid lines and decouples at the freeze-out points (full squares, triangles and star).

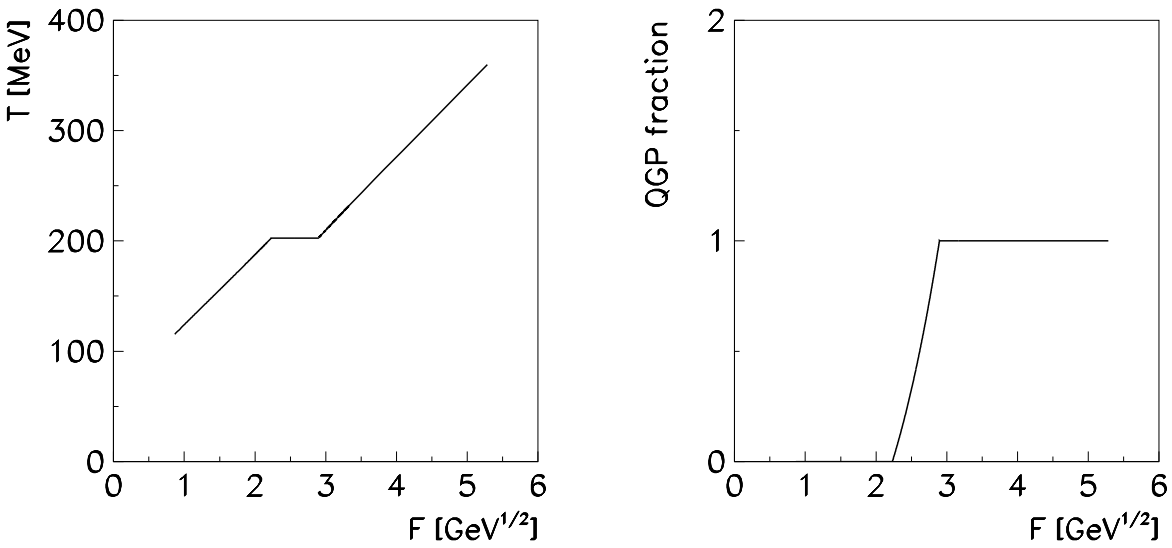

Figure 5. (a) The early stage (initial) temperature T of the fireball as a function of Fermi's energy variable F. (b) The fraction of volume occupied by the QGP as a function of F.

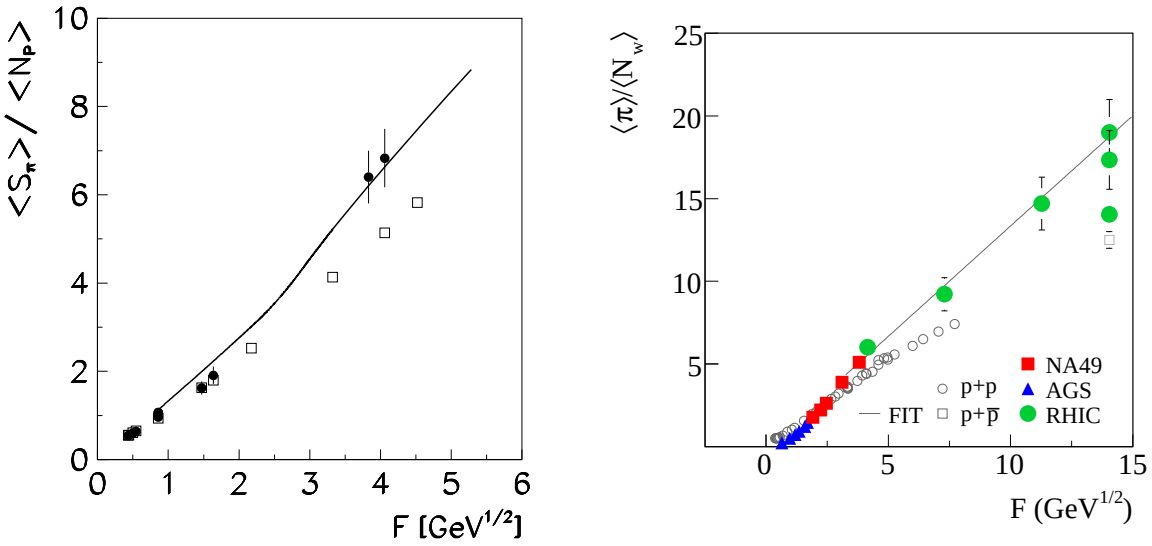

Figure 6. (a) The ratio $\langle S_\pi \rangle / \langle N_P \rangle$ as a function F. Experimental data on central collisions of two identical nuclei available in 1998 are indicated by closed circles. They are compared with SMES [4] calculations depicted by the solid line. The open boxes show results obtained for nucleon–nucleon interactions. (b) Energy dependence of the mean pion multiplicity per wounded nucleon measured in central PbPb and AuAu collisions (full symbols), compared to the corresponding results from $pp(\bar{p})$ reactions (open symbols). The compilation of data is from Ref. [5].

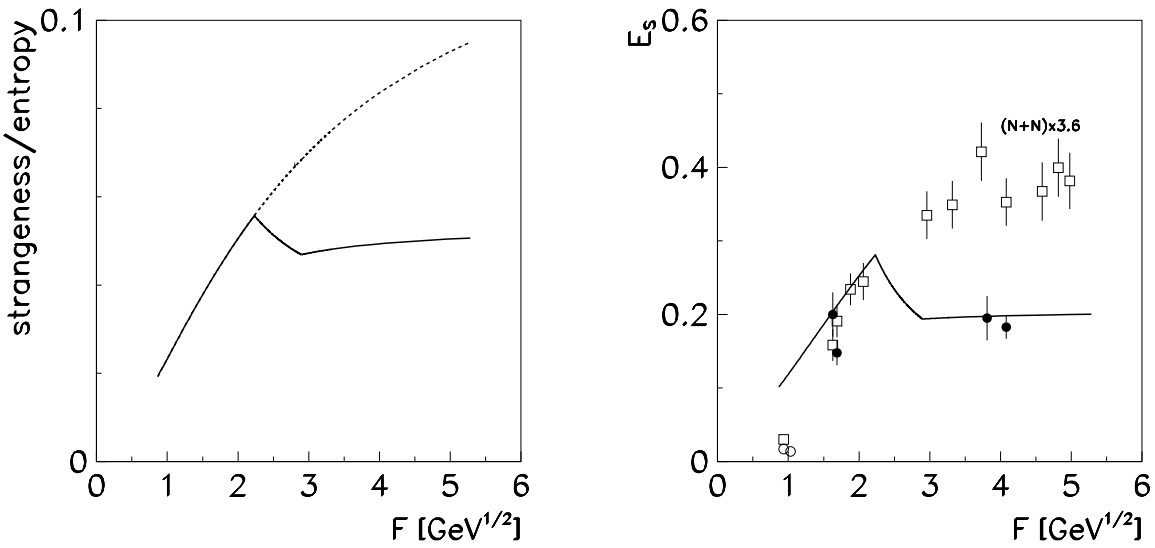

Figure 7. (a) The ratio of the total number of s and $\overline{s}$ quarks and antiquarks to the entropy (solid line) as a function of F [4]. The dashed line indicates the corresponding ratio calculated assuming absence of the phase transition to the QGP. (b) The ratio E_S as a function of F. Experimental data on central collisions of two identical nuclei available in 1998 are indicated by closed circles. These data should be compared with the SMES predictions [4] shown by the solid line. The open boxes show results obtained for nucleon–nucleon interaction, scaled be a factor 3.6 to match AA data at AGS energy.

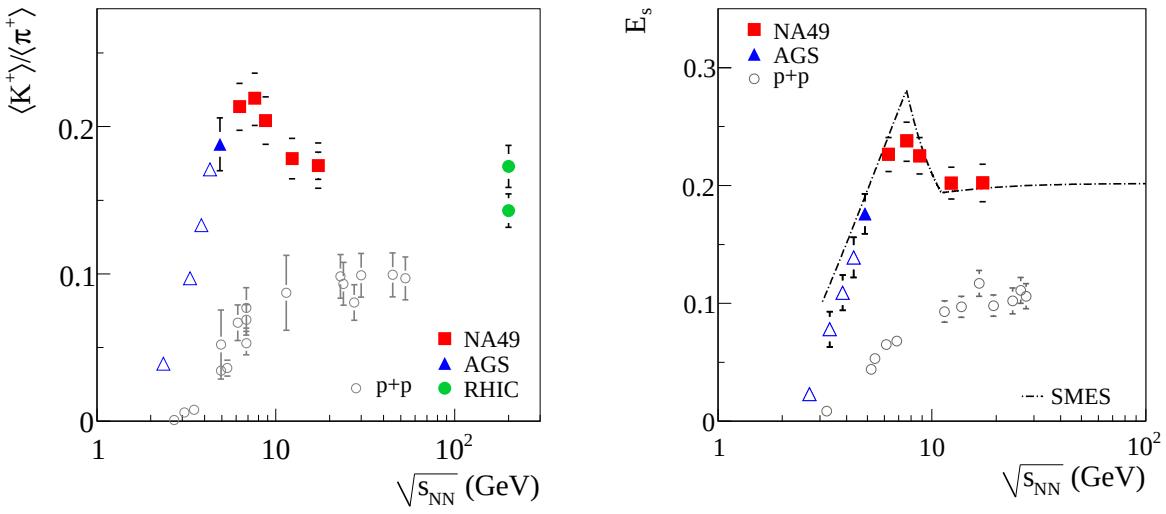

Figure 8. (a) Energy dependence of the ratio $\langle K^+\rangle/\langle\pi^+\rangle$ measured in central PbPb and AuAu collisions (full symbols) compared to the corresponding results from pp reactions (open circles). (b) Energy dependence of the relative strangeness production as measured by the E_s ratio (see text) in central PbPb and AuAu collisions (full symbols) compared to results from pp reactions (open circles). The compilation of data is from Ref. [5]. The dashed-dotted line in the figure shows the prediction of SMES [4].

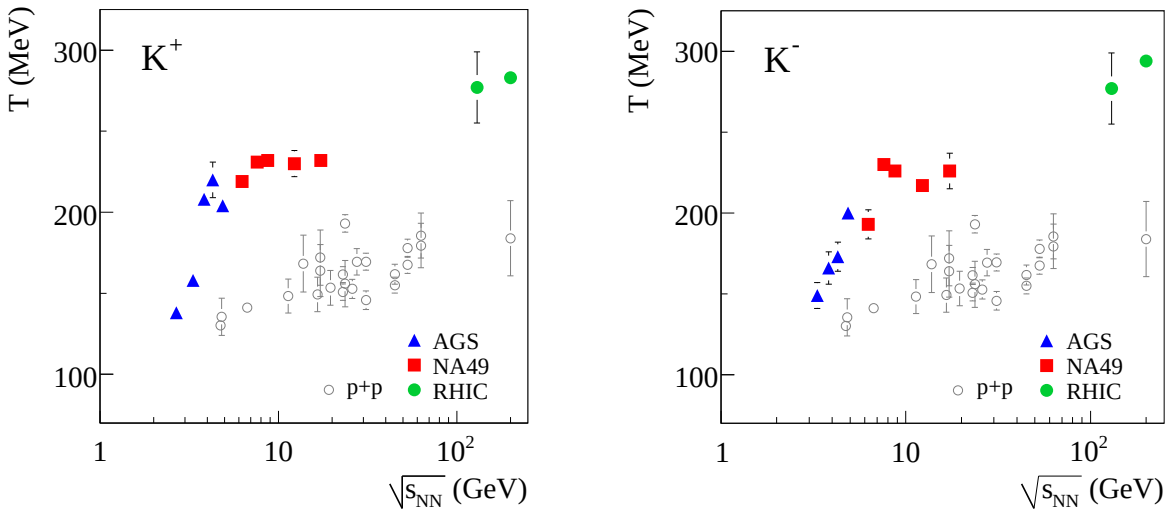

Figure 9. Energy dependence of the inverse slope parameter T^* of the transverse mass spectra of K^+ (a) and K^- mesons (b) measured at mid-rapidity in central PbPb and AuAu collisions. The $K^\pm$ slope parameters are compared to those from $p+p$ reactions (open circles). The compilation of data is from Ref. [5].

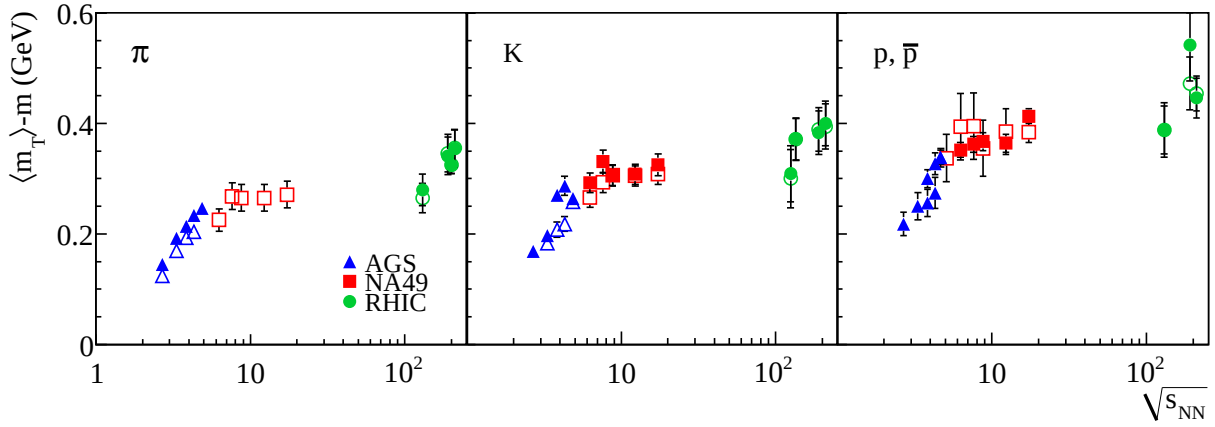

Figure 10. $\langle m_T \rangle - m$ for $\pi^\pm$ (a), $K^\pm$ (b), and p and $\bar{p}$ (c). In the plots, positively (negatively) charged hadrons are indicated by the full (open) symbols. The compilation of data is from Ref. [5].

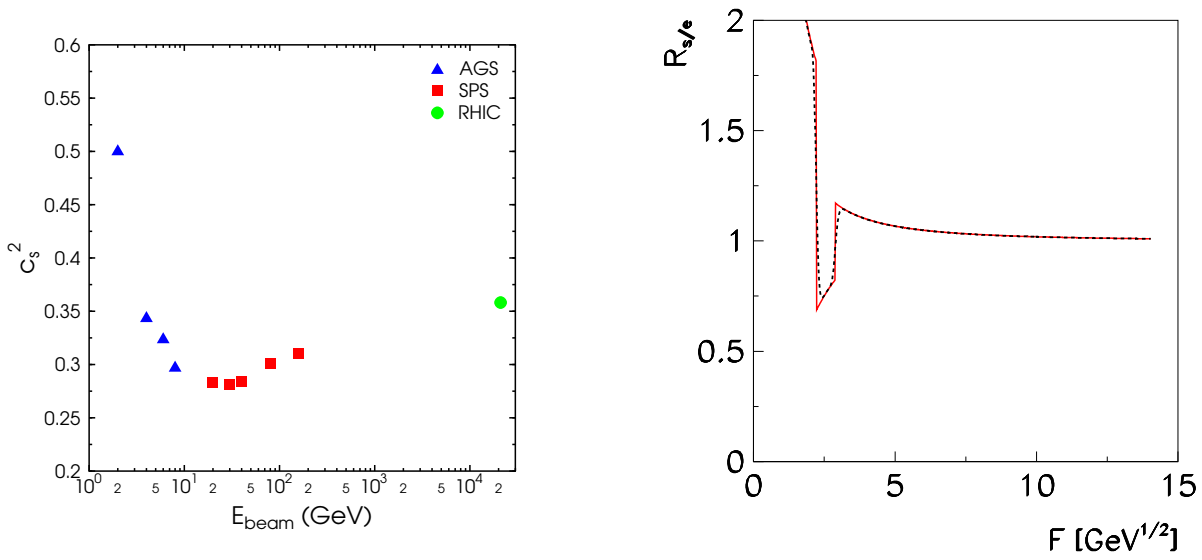

Figure 11. (a) Speed of sound as a function of beam energy for central PbPb (AuAu) reactions as extracted from the data using Eq. (6) [15]. (b) The *tooth* structure in the ratio of strangeness and entropy fluctuations $R_{s/e}$

FIGURE CAPTIONS

Fig. 1: Phases of water. When adding heat (energy) at constant pressure water is transformed from solid to liquid and then from liquid to vapor as indicated by the dashed arrow.

Fig. 2: Heating curve of water at fixed atmospheric pressure, corresponding to the trajectory in the phase diagram of water indicated by the dashed arrow in Fig. 1.

Fig. 3: Phases of strongly interacting matter. With increasing collision energy the matter created at the early stage of nucleus-nucleus collisions changes its properties as indicated by the arrow. At low energy it is in the confined phase (hadrons), at sufficiently high energy in the deconfined phase (QGP). M is the critical point of the nuclear liquid-gas phase transition. The shaded band shows the first order phase boundary between the hadron and QGP phase which is expected to end in a critical end point E. At E the sharp phase transition turns into a rapid crossover indicated as the dotted line.

Fig. 4: Parameters of strongly interacting matter created at the early stage of nucleus-nucleus interactions are shown by the full circles for central PbPb (AuAu) collisions at the top AGS energy ($\sqrt{s_{\rm NN}} \approx 5.5$ GeV), intermediate SPS energy ($\sqrt{s_{\rm NN}} \approx 7.6$ GeV) and top SPS energy ($\sqrt{s_{\rm NN}} \approx 17$ GeV). The created fireball expands and cools along trajectories indicated by solid lines and decouples at the freeze-out points (full squares, triangles and star).

Fig. 5: (a) The early stage (initial) temperature T of the fireball as a function of Fermi's energy variable F. (b) The fraction of volume occupied by the QGP as a function of F.

Fig. 6: (a) The ratio $\langle S_\pi \rangle / \langle N_P \rangle$ as a function F. Experimental data on central collisions of two identical nuclei available in 1998 are indicated by closed circles. They are compared with SMES [4] calculations depicted by the solid line. The open boxes show results obtained for nucleon–nucleon interactions. (b) Energy dependence of the mean pion multiplicity per wounded nucleon measured in central PbPb and AuAu collisions (full symbols), compared to the corresponding results from $pp(\bar{p})$ reactions (open symbols). The compilation of data is from Ref. [5].

Fig. 7: (a) The ratio of the total number of s and $\overline{s}$ quarks and antiquarks to the entropy (solid line) as a function of F [4]. The dashed line indicates the corresponding ratio calculated assuming absence of the phase transition to the QGP. (b) The ratio E_S as a function of F. Experimental data on central collisions of two identical nuclei available in 1998 are indicated by closed circles. These data should be compared with the SMES predictions [4] shown by the solid line. The open boxes show results obtained for nucleon–nucleon interaction, scaled be a factor 3.6 to match AA data at AGS energy.

Fig. 8: (a) Energy dependence of the ratio $\langle K^+\rangle/\langle\pi^+\rangle$ measured in central PbPb and AuAu collisions (full symbols) compared to the corresponding results from pp reactions (open circles). (b) Energy dependence of the relative strangeness production as measured by the E_s ratio (see text) in central PbPb and AuAu collisions (full symbols) compared to results from pp reactions (open circles). The compilation of data is from Ref. [5]. The dashed-dotted line in the Figure shows the prediction of SMES [4].

Fig. 9: Energy dependence of the inverse slope parameter T^* of the transverse mass spectra of K^+ (a) and K^- mesons (b) measured at mid-rapidity in central PbPb and AuAu collisions. The $K^\pm$ slope parameters are compared to those from $p+p$ reactions (open circles). The compilation of data is from Ref. [5].

Fig. 10: $\langle m_T\rangle - m$ for $\pi^\pm$ (a), $K^\pm$ (b), and p and $\bar{p}$ (c). In the plots, positively (negatively) charged hadrons are indicated by the full (open) symbols. The compilation of data is from Ref. [5].

Fig. 11: (a) Speed of sound as a function of beam energy for central PbPb (AuAu) reactions as extracted from the data using Eq. (6) [15]. (b) The *tooth* structure in the ratio of strangeness and entropy fluctuations $R_{s/e}$